A study of the effect of the longitudinal movement on the performance of small scale linear Fresnel reflectors

Arsenio Barbón [a], Luis Bayón [b, *], Covadonga Bayón-Cueli [c], Nicolás Barbón [a]

[a] Department of Electrical Engineering, University of Oviedo, Campus of Gijón, Spain
[b] Department of Mathematics, University of Oviedo, Campus of Gijón, Spain
[c] Polytechnic School of Engineering of Gijón, University of Oviedo, Spain

ABSTRACT

The sizing of a small-scale linear Fresnel reflector directly influences its primary cost as well as the annual energy output and, hence, its financial attractiveness. In addition, the area required for its installation is a critical parameter in most of the applications. This paper presents the analysis of the effects of the longitudinal movement on the performance of small-scale linear Fresnel reflectors. Our design, patented in year 2017, shows to be really innovative when compared to the existing designs shown in the literature. The three-movement option marks the novelty of the design. The effect of three parameters (i.e. energy absorbed by the absorber tube, primary cost, and reflector area ratio) is evaluated for two locations in Europe. Different configurations are analyzed and compared with the typical configuration of a large-scale linear Fresnel reflector. Numerical simulations were carried out using a MATLAB code to calculate the energy absorbed by the absorber tube, the primary cost, and the reflector area ratio. The comparison of the configurations provided insight into how latitude impacts on the results. It will be demonstrated that both the energy absorbed by the absorber tube and the primary cost increase with longitudinal movement, while the reflector area ratio decreases.

© 2019 Elsevier Ltd. All rights reserved.

1. Introduction

Concentrated Solar Power (*CSP*) is called to be a firm candidate for providing the majority of the renewable energy [1,2], and it can make a significant contribution to international commitments [3]. There are many possible configurations for *CSP*, such as the parabolic dish, linear Fresnel reflector (*LFR*), parabolic trough and central receiver. The *LFRs* have proven to offer a good solution due to their simplicity, robustness and low capital cost [4].

In the European Union (*EU*) households, heating and hot water alone account for 79% of total final energy use and cooling is a fairly small percentage of total final energy use [5]. Various types of solar concentrating collectors can be used for this purpose, for example the parabolic trough collectors [6,7] and the small-scale linear Fresnel reflectors (*SSLFR*). The *SSLFRs* have a lower efficiency (higher influence of the incidence angle and the cosine factor), lower maintenance (easier access for cleaning), lower structural requirements (rows of mirrors are mounted close to the ground and wind loads are substantially reduced), and a lower cost than the parabolic trough collectors [8].

There are numerous possible applications for the *SSLFRs*. These applications are mainly for industrial processes [9—11], low-temperature heat demand with high consumption rates: domestic water heating [12—14], heating/cooling of living space [15—17], and in the absorption of the cooled air in a Solar-GAX cycle [18]. There are also other applications, such as desalination [19], and daylighting systems [20].

A linear Fresnel reflector its characterized by: (i) the configuration of a 'conventional' central *LFR*, (ii) the use of stretched rows of mirrors, (iii) mirrors to reflect the sunlight to the focal line of an absorber tube, (iv) an absorber tube that runs longitudinally above the rows of mirrors located at a common focal line of the mirrors, (v) the absorber tube is specially coated so as to increase its capacity to absorb the incident solar radiation, (vi) the absorber tube is covered by a cavity receiver to reduce convective heat losses, (vii) the cavity receiver is sealed within the glass cover, (viii) rows of mirrors are located at the base of the *SSLFR*, and (ix) concentrated solar energy is transferred through the absorber tube into some thermal fluid capable of maintaining the liquid state at high

temperatures.

In large-scale and small-scale linear Fresnel reflectors, the rows of mirrors can be rotated on the north-south axis, so as to follow the sun's daily movement (elementary movement), in a way that they always reflect the sunlight on to the absorber tube. In large scale linear Fresnel reflectors the size of the rows of mirrors and the absorber tube does not permit any configuration allowing the modification of its position. These components are not provided with longitudinal movement. However, due to their dimensions some prototypes of small-scale linear Fresnel reflectors, allow certain movements which intend to enhance the energy absorbed by the absorber tube. For example, Dai et al. [21] describes three types of simultaneous movements: the elementary movement, the East-West translation of the entire reflector field according to the relative position of the Sun, and the rotation of a secondary reflector located in the receiver. Barbon et al. [22,23], also describes three types of simultaneous movements: the elementary movement, the East-West axis rotation of the mirror row, and the East-West axis rotation of the absorber tube. Zhu et al. [24], proposes a prototype with East-West orientation including both a reflective surface that forms a parabola and a receiver, which can move along the axial axis. Zhu et al. [25], also presents another prototype oriented in the East-West direction and rotated around the horizontal North-South axis, which has the possibility to adjust the tilt of the entire collector, according to the solar height.

The design proposed in Barbon et al. uses the movement of the mirror flied to minimize the end loss and the reflected light loss. On the other hand, Dai et al. [21], applies a translational movement to approach the same results. However, the design proposed in Barbon et al., reduces the required area for *SSLFR* installation. This is a key aspect of the design as, the roofs of the urban buildings are a logical location of the *SSLFRs*. In this case, the available area is a critical parameter. Moreover, it is necessary to take into account the building components (such as chimneys, elevator machine rooms, fans and plumbing vents). The building components reduce the available roof area for the *SSLFR* installation to a figure between 21% [26] and 30% of the roof real area [27]. The available roof area has in fact been identified as one of the main limiting factors in achieving zero energy buildings, especially for taller buildings [28].

Some other patented designs use other movements, apart from the elementary movement, in order to enhance the energy absorbed by the absorber tube [29,30].

In this paper we study the effects of the longitudinal movements in terms of energy absorbed by the absorber tube, primary cost, and surface required for installation. These parameters were calculated based on MATLAB codes especially developed for this study. For the shake of comparison, several geographic locations and configurations were studied, in order to evaluate the impact of the latitude in the results.

The analysis includes several configurations with longitudinal movements, to be compared with the classic large-scale LFR. We show the way the annual obtained energy and the required area vary as a function of the design parameters. We also study the primary cost, as we consider it to be a key factor when choosing the most beneficial option. The paper shows how some configurations based on the longitudinal movement significantly reduce the required area for the SSLFR installation, while increasing the obtained energy, and thus, showing a remarkable increase of our SSLFR design over the classic designs.

The paper is organized as follows. The components, parameters, and configurations of the *SSLFR* are described in Section 2. In Section 3, the parameters used in the comparative analysis are presented. Numerical simulations are presented in Section 4 for different configurations of the *SSLFR*. Finally, Section 5 summarizes the main contributions and conclusions of the paper.

Nomenclature	
A	Reflector area (m^2)
A_M	Mirror field area (m^2)
A_{effi}	Effective area of the absorber tube (m^2)
C_A	Primary cost of the assembly $(\euro)$
C_F	Primary cost of the foundation $(\euro)$
C_{FS}	Primary cost of the fixes structure $(\euro)$
C_{MS}	Primary cost of the mobile structure $(\euro)$
C_{MiS}	Primary cost of the movement system $(\euro)$
C_{MoS}	Primary cost of the mirrors system $(\euro)$
C_{SRS}	Primary cost of the secondary reflector system $(\euro)$
C_T	Total primary cost $(\euro)$
C_{TS}	Primary cost of the tracking system $(\euro)$
CL_g	Cleanliness factor of the glass
CL_m	Cleanliness factor of the mirror
D	Diameter of the absorber tube (m)
DNI	Direct Normal Irradiance (W/m^2)
d	Separation between two consecutive mirrors (m)
f	Height of the receiver (m)
IAF	Incidence angle modifier
L	Reflector length (m)
L_M	Length of the mirrors (m)
L_a	Length of the single absorber tube (m)
L_i	Position of $i-th$ mirror $(0 \leq i \leq n)$ (m)
L_a^l	Left length of the single absorber tube (m)
L_a^r	Right length of the single absorber tube (m)
n	Number of mirrors at each side of the central mirror
Q	Total power absorbed (W)
W	Mirror field width (W)
W_M	Width of the mirrors (m)
W_{ai}	Width illuminated on the absorber by the i-th by mirror (m)
α_b	Absorptivity of the absorber tube
α_i	Angle between the vertical at the focal point and the line connecting the centre point of each mirror to the focal point $(^o)$
α_S	Height angle of the Sun $(^o)$
β_a	Angle between the absorber tube and the horizontal plane $(^o)$
β_i	Tilt of i-th mirror $(^o)$
β_M	Angle between the mirror axis and the horizontal plane $(^o)$
γ_S	Azimuth of the Sun $(^o)$
δ	Declination $(^o)$
η_{opt}	Optical efficiency (%)
θ_l	Longitudinal incidence angle $(^o)$
θ_t	Transversal incidence angle $(^o)$
θ_z	Zenith angle of the Sun $(^o)$
λ	Latitude angle $(^o)$
ρ	Reflectivity of the primary mirrors
τ	Transmissivity of the glass

2. Technical considerations of an SSLFR

2.1. SSLFR components

The proposed *SSLFR*, designed with Autodesk Inventor as shown in Fig. 1, is composed of six main blocks: a fixed structure (1), mobile structure (2), primary reflector system (3), secondary reflector system (4), transmission systems (5) and tracking system (6). The primary reflector system is composed by multiple mirrors mounted on specially designed frames (7). The secondary reflector system (see Fig. 2) is formed by: absorber tube (8), cavity receiver (9), isolation (10), and glass covering (11). A prototype with these characteristics has been manufactured in a vocational training school (CIFP-Mantenimiento y Servicios a la Producción) in La Felguera, Asturias, Spain. A patent application for this prototype has been filed with the Spanish Patent and Brand Office [29].

The position of the mirrors and the absorber of the *SSLFR* can be adjusted using three different movements: Mirror Movement, movement of the secondary reflector system, and movement of the mobile structure. Fig. 3 shows the simplified schematic of these movements.
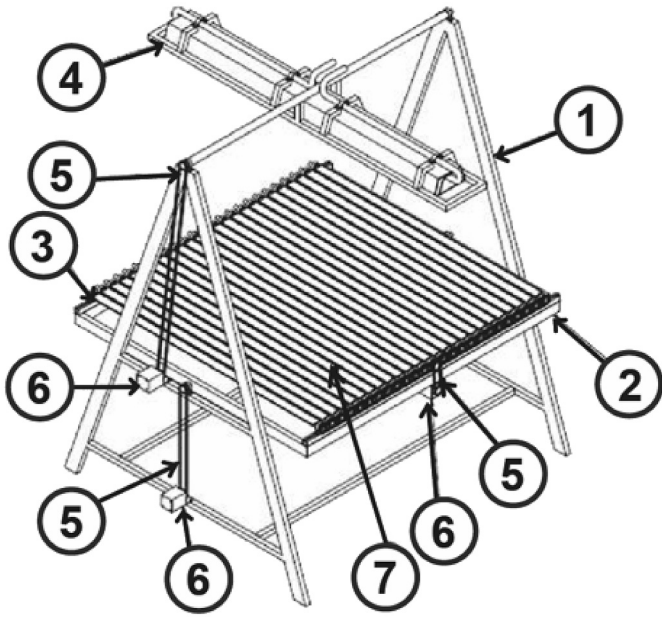
Fig. 1. SSLFR parts.
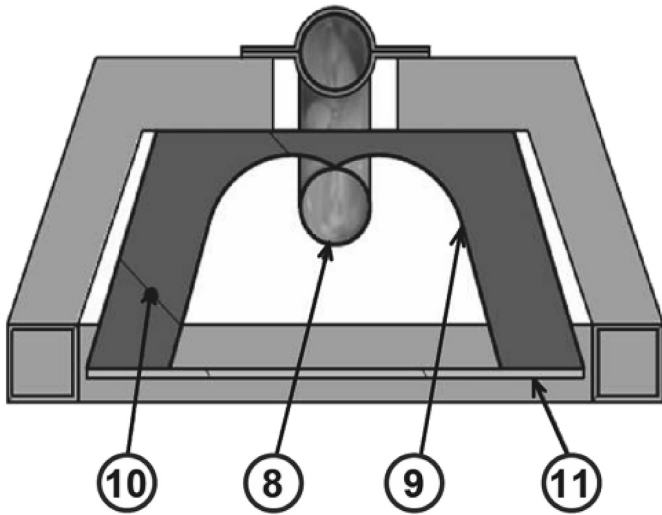
Fig. 2. Secondary reflector system.

Mirror movement, the mirrors can be rotated on the north-south axis, so as to follow the sun's daily movement. This movement requires $2 \cdot n + 1$ movement units. Movement of the mobile structure, the mirror row can be rotated on the east-west axis. Movement of the secondary reflector system, the receiver can also be rotated on the east-west axis. These movements require 2 additional movement units.

Each movement unit (see Fig. 4) includes: two bearings, two bearing supports, two shafts, a pinion gear, and the proportional part of the roller chain. Selected elements are as follows. Standard bearing type FAG 7205 B.TVP. Standard pinion gear with 19 tooth, step 3/8", module 3 (mm), and thickness 5 (mm). The bearing support consists of an 82.5 (mm) diameter stainless steel tube with a 20 (mm) wall thickness, and a $78 \times 28 \times 5$ (mm) stainless steel plate. The shaft consists of a 25 (mm) diameter carbon steel bar with a length of 150 (mm). The chain is a standard single strand, riveted, 6 (mm) size, roller chain.

The tracking algorithm can be implemented in a controller based on a Raspberry Pi 3, due to its low cost, compact size, compatibility and easy interfacing. The Raspberry Pi 3 is a single board computer based on a 900 MHz quad-core ARM Cortex-A7 CPU, with 1 GB RAM, 40 GPI/O pins, 4 USB ports, Full HDMI port, Ethernet port, and a Micro SD card slot. A total of three stepper motors and drivers are required, since the position of the mirrors and the absorber of the *SSLFR* can be adjusted using three different movements. Each driver supplies appropriate control signals and supply voltage to the associated stepper motor. The system requires additional sensors such as: wind sensor, encoder, limit switches.

The assumptions made in this study are as follows:

(i) Mobile structure. In this system, the tracking error and misalignment are not considered.
(ii) Primary reflector system. The pivoting point of each mirror coincides with the central point of the mirror; hence, it is always focused on the central point of the absorber tube. The mirrors are flat and specularly reflecting. The mirrors have the same length and width.
(iii) Secondary reflector system. A single absorber tube is used.
(iv) Transmission systems. The tracking error and misalignment are not considered in these systems.
(v) Tracking system. The mobile structure, secondary reflector system, and primary reflector system are perfectly tracked so as to follow the apparent movement of the Sun.

2.2. SSLFR parameters

Fig. 5, Fig. 6 and Fig. 7 show the simplified schematics of a generic *SSLFR*. The accurate calculation of an *SSLFR* requires the precise identification of parameters specific to the solar concentrator under study. In order to do that, the angle of incidence of the solar radiation is separated into two projection planes (see Ref. [31]). This consideration divides the analysis into transversal and longitudinal studies [22]. In addition, it defines two angles that will be significant for the design of the *SSLFR*: the transversal incidence angle (θ_t) and the longitudinal incidence angle (θ_l). The transversal incidence angle (θ_t) is defined as the angle between the vertical and the projection of the sun vector on the East-West plane (the plane orthogonal to the absorber tube), and the longitudinal incidence angle (θ_l) is defined as the angle between the vertical and the projection of the sun vector on the North-South plane. These angles are required to calculate the parameters of the *SSLFR*. These definitions are valid when the *SSLFR* is aligned horizontally and the absorber tube aligned in the North-South orientation. The relative position of the Sun with respect to the *SSLFR* is determined using the known Solpos algorithm [32]. The parameters associated with each study are shown below.

The parameters used in the transversal study are as follows: n is the number of mirrors at each side of the central mirror (the total number of mirrors of the *SSLFR* is $2n + 1$), W_M is the mirror width, d is the separation between two consecutive mirrors, D is the diameter of the absorber tube, and f is the height of the receiver. From these parameters the following are obtained: L_i is the position with respect to the central mirror of the $i - th$ mirror ($0 \leq i \leq n$), β_i is the mirror tilt of $i - th$ mirror ($0 \leq i \leq n$), α_i is the angle between the vertical at the focal point and the line connecting the centre point of each mirror to the focal point ($0 \leq i \leq n$), and W_{ai} is the illuminated width on the absorber tube by the $i - th$ mirror.

The parameters used in the longitudinal study are: β_M is the angle between the mirror axis and the horizontal plane, β_a is the angle between the absorber tube and the horizontal plane, θ_z is the
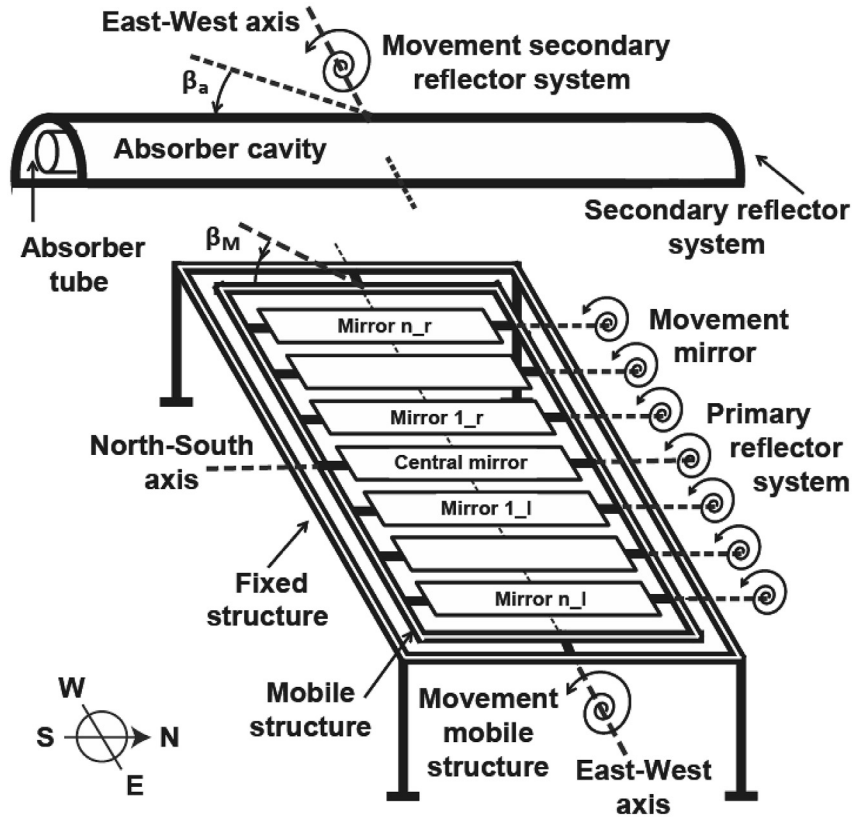
Fig. 3. Schematic of the three movements of an SSLFR.
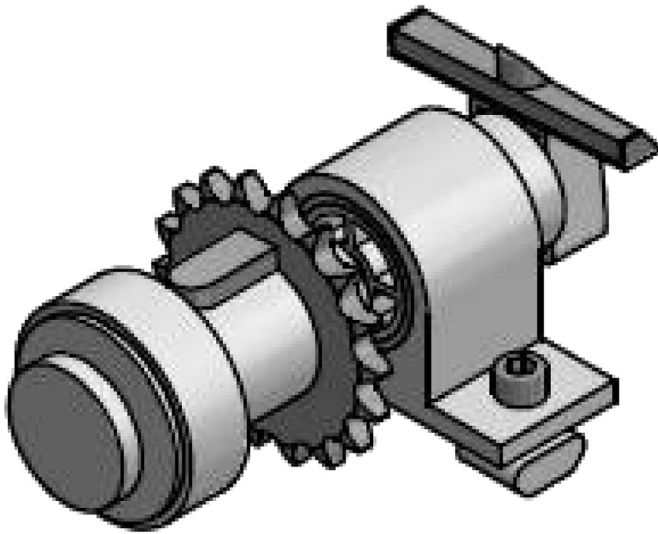
Fig. 4. Movement unit.

zenithal solar angle, L_M is the mirror length, L_a is the total length of the single absorber tube, L_a^l is the left length of the single absorber tube, and L_a^r is the right length of the single absorber tube ($L_a = L_a^l + L_a^r$).

By relating some of the parameters listed above, one can determine which parameters will be used for the design, i.e: mirror field width (W), mirror field area (A_M), reflector length (L), and reflector area (A).

The mirror field width can be calculated as:

$$W = 2 \cdot n \cdot (W_M + d) + W_M \tag{1}$$

The mirror field area can be calculated as:

$$A_M = W \cdot L_M \tag{2}$$

The reflector length can be calculated with the following relations:

$$L = \begin{cases} L_M\cos(\beta_M) & \text{if} & \begin{bmatrix} L_a^l\cos(\beta_a) \le \frac{1}{2}L_M\cos(\beta_M) \\ \& \\ L_a^r\cos(\beta_a) \le \frac{1}{2}L_M\cos(\beta_M) \end{bmatrix} \\ L_a^l\cos(\beta_a) + \frac{1}{2}L_M\cos(\beta_M) & \text{if} & \begin{bmatrix} L_a^l\cos(\beta_a) > \frac{1}{2}L_M\cos(\beta_M) \\ \& \\ L_a^r\cos(\beta_a) \le \frac{1}{2}L_M\cos(\beta_M) \end{bmatrix} \\ \frac{1}{2}L_M\cos(\beta_M) + L_a^r\cos(\beta_a) & \text{if} & \begin{bmatrix} L_a^l\cos(\beta_a) \le \frac{1}{2}L_M\cos(\beta_M) \\ \& \\ L_a^r\cos(\beta_a) > \frac{1}{2}L_M\cos(\beta_M) \end{bmatrix} \end{cases} \tag{3}$$

The reflector area can be calculated as:
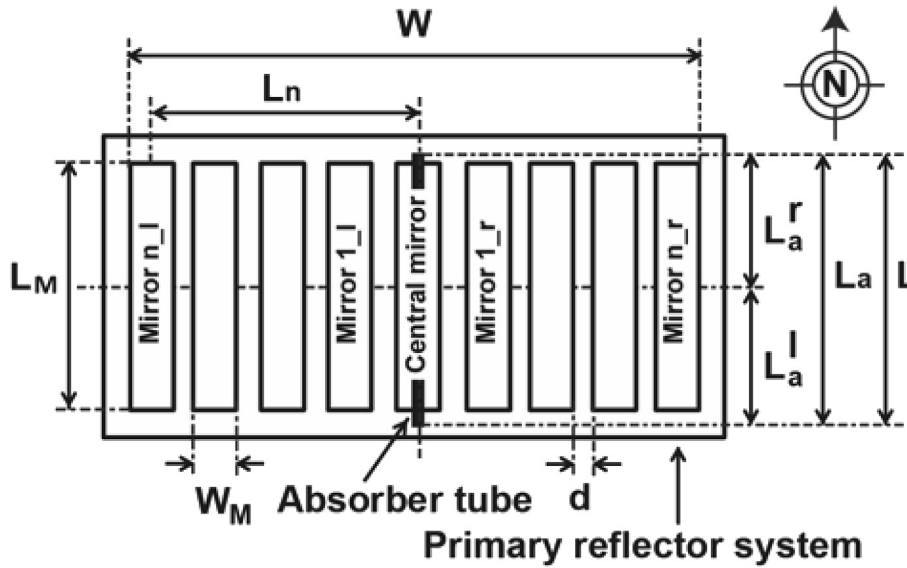
Fig. 5. Schematic top view of an SSLFR.
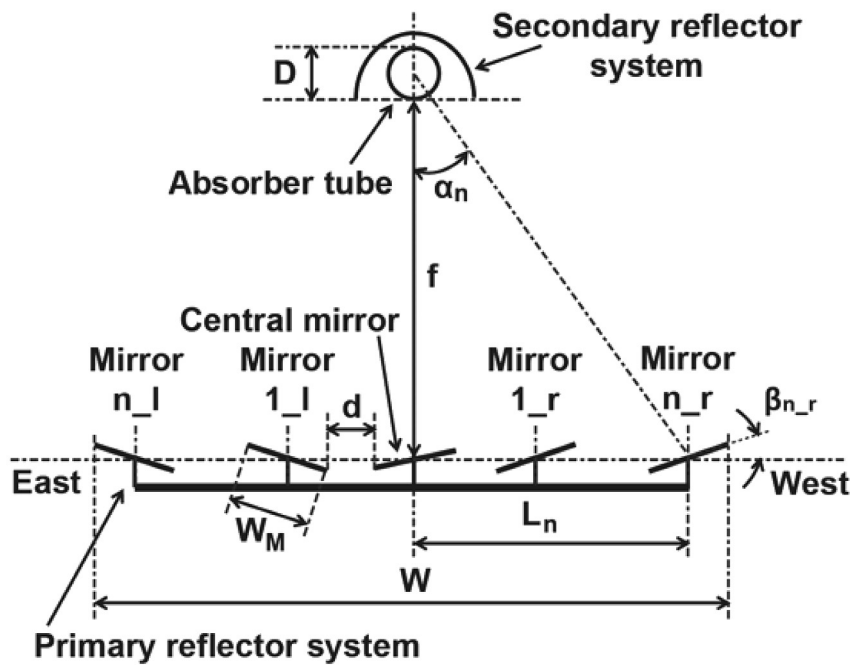
Fig. 6. Schematic front view.

$$A = W \cdot L \tag{4}$$

2.3. SSLFR configurations

It is necessary to define some configurations that allow us to perform an adequate analysis. In order to define the configurations we have evaluated if the mobile structure and the secondary reflector system have longitudinal movement or not. With these premises one can obtain several combinations. These considerations are also interesting to analyze the effect of the latitude on this study. Using the prototype, a high number of configurations can be studied, for the relative position between the primary reflector system and the secondary reflector system. Table 1 shows 7 designs of possible configurations.

As it can be seen in Table 1, when working with the configuration C_1, not the mobile structure neither the secondary reflector system have longitudinal movement and they are parallel with the horizontal plane. This configuration will be used as a basis for future comparisons as it is used in large-scale linear Fresnel reflectors. In the configurations C_2, C_3, and C_4, the design ensures that for any time of the day the rays reflected by the mirrors in the longitudinal direction are always vertical to the tube, varying the angle of incidence on the absorber tube for each of these configurations. When working in C_2, the secondary reflector system has
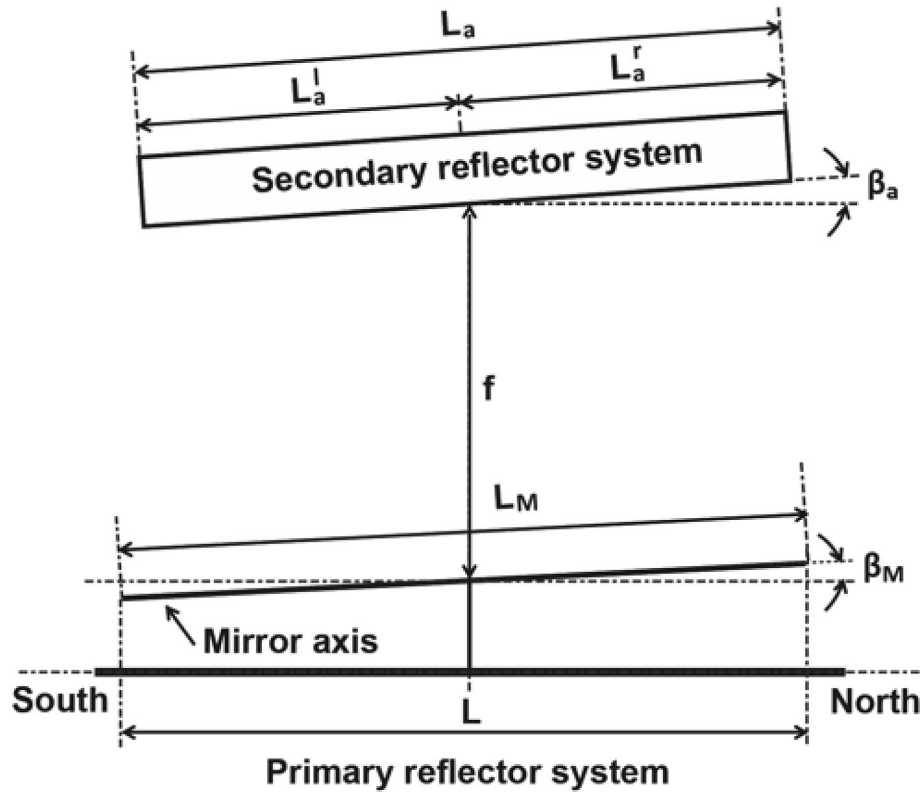
Fig. 7. Schematic side view.

Table 1
Configurations under study.

Configuration	Mobile structure		Secondary reflector system	
	$\beta_M(°)$	Motion	$\beta_a(°)$	Motion
C_1	0	No	0	No
C_2	$\theta_z/2$	Yes	$\theta_z/2$	Yes
C_3	$\theta_z/2$	Yes	λ	No
C_4	$\theta_z/2$	Yes	0	No
C_5	$\lambda - \delta$	Yes	$\lambda - \delta$	Yes
C_6	$\lambda - \delta$	Yes	λ	No
C_7	$\lambda - \delta$	Yes	0	No

the same longitudinal movement as the mobile structure. In C_3, the secondary reflector system is not provided with longitudinal movement and forms an angle of λ with the horizontal plane. On the other hand, in C_4, the secondary reflector system is parallel to the horizontal plane and it is not provided with longitudinal movement. The configuration that obtains better total obtained energy, keeping the *SSLFR* parameters constant, is configuration C_2 [23].

The design of a single axis polar solar tracker is used as the base configuration, inspiring the values in configuration C_5. These trackers rotate on an axis oriented in the North-South direction at an axial inclination equal to the latitude of the place, sometimes corrected by means of the declination. Thus, the axis of rotation of the system is parallel to the Earth axis. A single axis polar solar tracker can reach efficiencies of over 96% compared to systems with two axes. Changing some parameters of the base configuration, the configurations C_6 and C_7 are obtained. In C_5, the secondary reflector system and the mobile structure have the same longitudinal movement. In configurations C_6 and C_7 there is no longitudinal

movement on the secondary reflector system. In C_6 the secondary reflector system forms an angle of λ with the horizontal plane. Finally, in configuration C_7 the secondary reflection system is parallel to the horizontal plane.

There is a major difference between configurations C_2, C_3, and C_4 and configurations C_5, C_6, and C_7. In the first group, the movement occurs throughout the day, while in the second group the movement is performed once a day.

Other configurations have been studied and discarded due to the low energy obtained.

The longitudinal movement of the mobile structure influences on the mirror length. It is interesting to know the value that L_M can take for each configuration, in order to compare it with the mirror length of the configuration C_1, L_M^{C1}. To obtain this value, the minimum values of angle between the mirror axis and the horizontal plane, $\beta_M$min, need to be calculated. Table 2 shows these values (see Fig. 5).

Also, the longitudinal movement of the mobile structure or/and the secondary reflector system have influence on of the length and position of the absorber tube (L_a, L_a^l, L_a^r). The algorithm proposed by Ref. [23] can be used for an appropriate determination of optimal values of L_a, L_a^l, and L_a^r. This algorithm allows the optimization of the position and length of the absorber tube based on the

Table 2
Influence of mobile structure movement on L_M.

Configuration	Mirror length	$\beta_M$min(°)	Day	Solar time
C_2, C_3, C_4	$L_M = \dfrac{L_M^{C1}}{\cos(\beta_{M\min})}$	$\theta_z/2$	June 21 st	12:00
C_5, C_6, C_7	$L_M = \dfrac{L_M^{C1}}{\cos(\beta_{M\min})}$	$\lambda - (23.45)$	June 21 st	No influye

longitudinal design. The method is based on a geometrical algorithm that minimizes the area between two curves, minimizing the end loss and reflected light loss, which are now taken into consideration.

3. Parameters used for the comparison

In other to perform an adequate comparative analysis the relevant parameters have to be identified and defined to assess each of the suggested configurations. These analyses are based on configuration C_1, as it is the typical configuration of a large-scale linear Fresnel reflector. For this reason, it is considered that L_M^{C1}, W_M, d and n, remain constant.

The available area for the installation of the $SSLFR$ divides the study into two cases: (i) the available area is not a critical parameter, and (ii) the available area is a critical parameter. The evaluation of each of the configurations is carried out by means of the annual energy absorbed by the absorber tube and the primary cost, if the available area is not a critical parameter. If the available area is a critical parameter the evaluation will include the reflector area ratio. These parameters are defined as follows.

3.1. Energy absorbed by the absorber tube

The power absorbed by the absorber tube of an $SSLFR$ can be calculated as [33]:

$$Q = \sum_{i=0}^{2 \cdot n} DNI \cdot \eta_{opt} \cdot IAF_i \cdot A_{effi} \qquad (5)$$

where these parameters are:

(i) DNI is the direct normal irradiance.
(ii) η_{opt} is the total optical yield, which is calculated considering the reflectivity of the mirrors (ρ), the cleanliness factors of the mirror (CI_m) and of the glass covering the secondary absorber (CI_g), the transmissivity of this glass (τ), and the absorptivity of the material of which the absorber tube is made (α_b). Although some of these parameters, especially τ, should change with the angle of incidence (see Ref. [34]), in this study they are considered constant for simplicity (see Refs. [35,36]). These values are: $\rho = 0.94$ (see Ref. [34]); $CI_m = CI_g = 0.96$ (see Ref. [37]); $\tau = 0.87$ if $\alpha_i \leq 20°$, $\tau = 0.85$ if $20° \leq \alpha_i \leq 30°$ (see Ref. [38]).
(iii) IAF_i considers the variation in the optical performance of an $SSLFR$ for varying ray incidence angles, by the i-th mirror [33].

(iv) A_{effi} is the effective area of the absorber tube by the i-th mirror that is actually illuminated [33].

3.2. Primary cost

The methodology proposed by Ref. [39] will be applied in order to obtain the primary cost. Following the steps of that methodology, the study of the primary cost has been divided into the following elements: fixed, mobile structure, movement system, mirror system, secondary reflector system, tracking system, assembly, and foundation. The primary cost equation for each element is listed in Table 3 [39].

The total primary cost C_T of an $SSLFR$ is given by the sum of the individual costs of the eight components listed above:

$$C_T = C_{FS} + C_{MS} + C_{MoS} + C_{MiS} + C_{SRS} + C_{TS} + C_A + C_F \qquad (6)$$

3.3. Reflector area ratio

The reflector area ratio is defined as the ratio between the area required for the $SSLFR$ installation (m^2) and the annual energy absorbed by the absorber tube (MWh):

$$RAR = \frac{A}{E} \qquad (7)$$

4. Results and discussion

In this section, the results of a large number of numerical simulations, that were performed using a MATLAB code are presented. The aim is to estimate the effect of the longitudinal movement on various parameters like the annual energy absorbed by the absorber tube, the primary cost, and the reflector area ratio. These parameters are analyzed for several geographic locations and configurations.

All the calculations are based on a sub-hourly distribution of the direct normal irradiance for each specific geographic location: Almeria (Spain), with latitude $36°50'07''N$, longitude $02°24'08''W$ and altitude 22 (m) and Berlin (Germany), with latitude $52°31'27''N$, longitude $13°24'37''E$ and altitude 37 (m). A derived database and system integrating data (PVGIS) [40] were used to estimate the solar irradiance. Numerical simulations were performed using a MATLAB code. The developed code incorporates sub-routines, discretized every 10 min, to calculate: DNI, mirror

Table 3
Primary cost.

Element	Cost
Fixed structure	$C_{FS} = W_{FS} \cdot k^{St}$
Mobile structure	$C_{MS} = W_{MS} \cdot k^{St} + L_{rail} \cdot k^R$
Movement system	$C_{MoS} = (2 \cdot n + a) \cdot k^{MoU}$
Mirror system	$C_{MiS} = (2 \cdot n + 1) \cdot k^{MiU}$
Secondary reflector	$C_{SRS} = W_{AT} \cdot k^{AT} + A_{CR} \cdot k^{CR} + A_I \cdot k^I + A_{GC} \cdot k^{GC} + W_{SRSS} \cdot k^{St} + A_{PC} \cdot k^{PC} + L_{shaft\ SRS} \cdot k^{shaft\ SRS}$
Tracking system	$C_{TS} = a \cdot k^{MD} + k^C + k^{Se}$
Assembly	$C_A = (2 \cdot n + a) \cdot k^A$
Foundation	$C_F = V_F \cdot k^F$

where C_{FS} is the primary cost of the fixed structure (€), C_{MS} is the primary cost of the mobile structure (€), C_{MoS} is the primary cost of the mirrors system (€), C_{MiS} is the primary cost of the movement system (€), C_{SRS} is the primary cost of the secondary reflector system (€), C_{TS} is the primary cost of the tracking system (€), C_A is the primary cost of the assembly works (€), and C_F is the primary cost of the foundation (€). Several cost parameters are proposed to be defined as the sum of the material, the labor and tooling cost. The rest of parameters can be consulted in Ref. [39].

position, IAF, L_{ai}, and l_a. The shading, blocking, and end loss effects were also taken into account.

The seven configurations described in this paper were considered for this analysis (see Table 2). The parameters listed in Table 4 (see Refs. [22,23,33] [24,25,39]), remain constant in all the configurations.

Table 5 shows the values of β_{Mmin} and mirror length for all the configurations (see Table 2). It is remarkable that, for the same available length (2.00 m), configurations C_2, C_3, C_4 and C_5, C_6, C_7 allow the use of longer mirror lengths due to the longitudinal movements, which leads, as discussed later, to a notable increase of the energy obtained.

The longitudinal position and length of the absorber tube are two critical parameters for the design of an $SSLFR$. Using non-optimal values leads to decreases of up to 80% in the energy produced [33]. Therefore, in an $SSLFR$ the longitudinal optimization is essential. The longitudinal optimization involves the calculation of the optimal values of the total length, left length, and right length of the absorber tube (L_a, L_a^l, and L_a^r respectively). The algorithm proposed by Ref. [23] will be used to determine the optimal values of L_a, L_a^l, and L_a^r. This algorithm allows the optimization of the position and the length of the absorber tube based on the longitudinal design. This method is based on a geometrical algorithm that minimizes the area between two curves, thereby minimizing the end loss and reflected light loss, which are now taken into consideration. Table 6 presents the values obtained by the optimization of the length and position of the absorber tube (with the sign convention adopted, lengths from the centre of the mirror to the left are considered positive, and those to the right, negative). This table shows the influence of the longitudinal movement on the parameters, and how L_a increases or decreases. An increase in L_a leads to an increase of the area required for the $SSLFR$ installation and the primary cost.

Table 4
Parameters constants used in the study.

	Parameters	Value
n	Number of mirrors at each side of the central mirror	12
W_M	Mirror width	0.06 (m)
d	Separation between two consecutive mirrors	0.024 (m)
D	Diameter of the absorber tube	0.0486 (m)
f	Height of the receiver	1.50 (m)
W	Mirror field width	2.076 (m)

Table 5
Mirror length for all the configurations.

Configuration	Almeria		Berlin	
	$\beta_{Mmin}(°)$	L_M (m)	$\beta_{Mmin}(°)$	L_M (m)
C_1	0	2.00	0	2.00
C_2, C_3, C_4	6.69	2.01	14.53	2.07
C_5, C_6, C_7	13.39	2.05	29.07	2.29

Table 6
Optimization of the length and position of the absorber tube.

Configuration	Almeria			Berlin		
	L_a^l	L_a^r	L_a	L_a^l	L_a^r	L_a
C_1	−0.037	−2.037	2.00	−0.865	−2.865	2.00
C_2	1.005	−1.005	2.01	1.035	−1.035	2.07
C_3	1.190	−1.190	2.380	1.524	−1.524	3.048
C_4	0.953	−0.953	1.906	0.927	−0.927	1.854
C_5	1.897	−0.152	2.050	2.309	0.019	2.29
C_6	1.912	−0.166	2.078	2.319	0.021	2.298
C_7	2.394	−0.194	2.589	3.857	0.049	3.807

In configuration C_4, the longitudinal movement of the mobile structure leads to an approximate decrease in 5% and 8% of L_a, in Almeria and Berlin, respectively. On the other hand, in configuration C_3, the longitudinal movement of the mobile structure leads to an increase of approximately a 20% and 53% of L_a, in Almeria and Berlin, respectively. The influence of the latitude of the geographic location is very remarkable when working with this configuration. The comparison of these two configurations shows the influence of the inclination of the secondary reflector system in the way L_a increases. In configuration C_2, the two longitudinal movements lead to similar results to those obtained with configuration C_1, but with the lengths centered with respect to the $SSLFR$ centre. In C_2, C_3, and C_4 increasing the latitude does not modify the displacement of the absorber tube, as the latitude has no impact on the longitudinal movement.

In configuration C_7, the longitudinal movement of the mobile structure implies an increase in L_a of approximately a 30% and a 90%, in Almeria y Berlin, respectively. When working with these configurations the influence of the latitude of the geographic location under study is very remarkable. In configuration C_6, the longitudinal movement of the mobile structure leads to an increment of approximately 4% and 15% in L_a, for Almeria y Berlin, respectively. Comparing these results, it is clear that the secondary reflector system inclinations has influence in the way L_a diminishes. In configuration C_5, having two longitudinal movements gives similar results to those obtained in the configuration C_6. Finally, in C_5, C_6, and C_7 as the latitude increases the absorber tube suffers a displacement in the South direction, due to the dependency of the longitudinal movement on the latitude.

Table 7 shows the annual energy absorbed by the absorber tube and the reflector area ratio, for each configuration, in Almeria and Berlin.

In Table 8 the primary costs are displayed, in percentage terms with respect to the base ones of configuration C_1, for each configuration, in Almeria and Berlin. As the cost parameters significantly vary depending on the manufacturing country, they are represented with respect to the results of C_1 for each geographic location, for the sake of comparison. The parameters considered for this analysis are presented in Ref. [39]. The increase in the primary cost of all the configurations with respect to the primary cost of C_1, can be explained as: (i) an increase in the primary cost of the mirror system due to the increase in the length of the mirror, (ii) an

Table 7
Annual energy and RAR.

Configuration	Annual energy (MWh)		RAR (m^2/MWh)	
	Almeria	Berlin	Almeria	Berlin
C_1	8.17	4.12	0.77	1.94
C_2	9.53	5.68	0.43	0.73
C_3	10.30	7.25	0.40	0.57
C_4	8.80	5.12	0.47	0.81
C_5	7.43	5.75	0.79	1.09
C_6	7.83	6.16	0.67	0.81
C_7	8.44	7.54	0.83	1.33

Table 8
Primary cost.

Configuration	Almeria	Berlin
C_1	100.00	100.00
C_2	110.69	112.10
C_3	110.09	119.10
C_4	104.16	104.12
C_5	111.69	116.07
C_6	106.26	108.42
C_7	112.63	126.16

increase of the primary cost of the secondary reflector system due to the increase of the length of the absorber tube and thus an increase of the rest of components, (iii) an increase in the primary cost of the tracking system due to the implementation of longitudinal movements, and (iv) an increase in primary cost of the movement system due to the inclusion of longitudinal movements (although point (iv) can be neglected).

4.1. Effects on the annual energy absorbed by the absorber tube and primary cost

In this study the available area is not a critical parameter. The comparison is being done based on the configuration C_1, typical configuration for large-scale linear Fresnel reflectors.

Fig. 8 shows the percentages, with respect to configuration C_1, of the annual energy absorbed by the absorber tube and primary cost, for each configuration, in Almeria.

Configurations whose longitudinal movements allow the rays reflected by the mirrors in the longitudinal direction to be always vertical for any time of day (C_2, C_3, C_4), show better annual energy results with a moderate increase on the primary cost. As it can be seen, the best behavior is obtained in configuration C_3. Comparing the results obtained for configurations C_3 and C_4, shows the influence of the secondary reflector system inclination on the annual energy obtained. As the inclination increases the total annual energy increases, so does the primary cost in a moderate pace.

The configurations whose longitudinal movements depend on the latitude, (C_5, C_6), show worse results than the configuration C_1, however C_7 shows slightly better results. The worst behavior is shown when two longitudinal movements are allowed (configuration C_5). The differences in the results of C_6 and C_7, are based on the influence of the secondary reflector system inclination on the design. An increase on the inclination of the secondary reflector system implies a decrease of the annual energy, and the primary cost.

Fig. 9 shows the results for each configuration in Berlin. Once again, the results of configuration C_1 have been taken as the base. In configurations C_2, C_3, C_4 the longitudinal movement positively
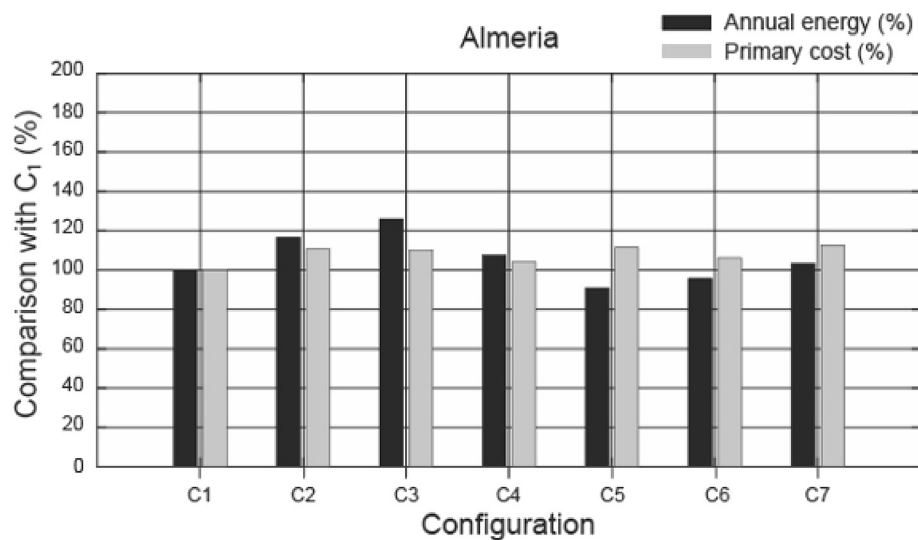
Fig. 8. Comparison with configuration C_1, in Almeria.
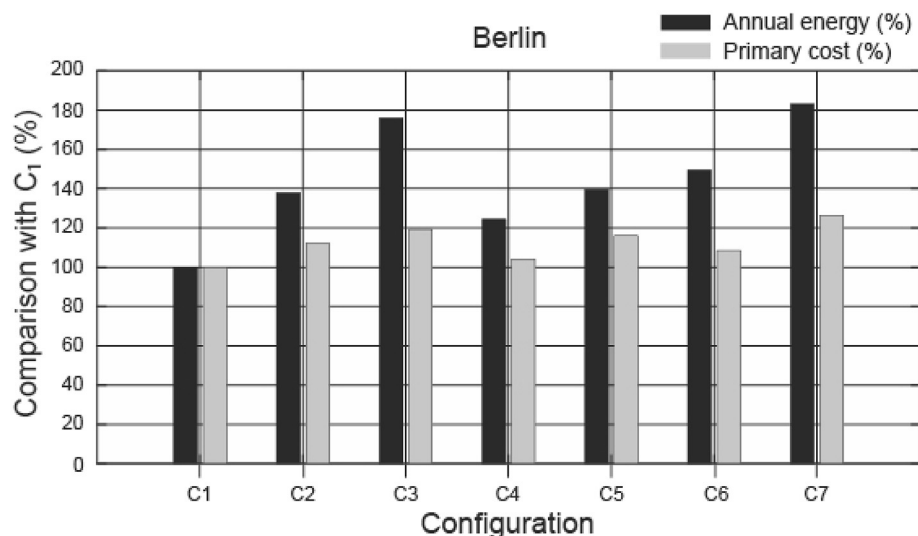
Fig. 9. Comparison with configuration C_1, in Berlin.

affects the annual energy results, with a notable increase in primary cost. These configurations verify that, for any time of the day, the rays reflected by the mirrors in the longitudinal direction are always vertical. In terms of annual energy, the best results are obtained for C_3, but this configuration also has the highest primary cost of these group. The inclination of the secondary reflector system allows to obtain greater amounts of annual energy, with a higher primary cost. This is the main difference between the configurations C_3 and C_4.

The longitudinal movements have positive effects on the annual energy when working with configurations C_5, C_6 and C_7 as well, where the movements depend on the latitude. Configuration C_7 obtains the best results for the annual energy, with the biggest primary costs. C_5 shows the worst behavior, even though it allows two longitudinal movements. In these cases the increase of the inclination of the secondary reflector system, implies a decrease of the annual energy, and the primary cost. The influence of the inclination can be seen by comparing the results of C_6 and C_7.

The configurations that allow two longitudinal movements (configuration C_2 and C_5) do not obtain better results of the annual energy and they imply an increment in primary cots. The best behavior is obtained for configuration C_3, both in Almeria and Berlin. The configurations whose longitudinal movements depend directly on the latitude obtain better results as the latitude of the geographic location increases.

4.2. Effect on the area required for SSLFR installation

There are situations where the available area is the critical parameter for the installation of the *SSLFR* [41]. For the sake of the comparison, the results of each configuration are compared with those of configuration C_1, typical configuration of a large-scale linear Fresnel reflector. Fig. 10 shows, the reflector area ratio, for each configuration, in Almeria and in Berlin, expressed as the percentage with respect to C_1.

The area required for the *SSLFR* is significatively reduced when working with configurations whose longitudinal movements allow the reflected rays by the mirrors in the longitudinal direction to be always vertical, for any time of day (C_2, C_3, C_4), showing better results in Berlin than in Almeria. Regardless of the location, configuration C_3 shows the best behavior. The differences between the results C_3 and the second-to-best configuration (C_4) reflect how

the inclination of the secondary reflector system influences the required area. As the inclination of the secondary reflector system increases, less area is required for the *SSLFR* installation.

Both in Almeria and in Berlin, the worst results are obtained when working with configurations where the longitudinal movements depend on the latitude (C_5, C_6, C_7). As it can be seen in Fig. 10 the results are notably worst in Almeria, where C_7 shows the worst performance of all the configurations. Configurations C_6 and C_7, reflect how the inclination of the secondary reflector system affect the results. An increase in the inclination on the secondary reflector system leads to a decrease in the required installation area, both in Almeria and in Berlin.

5. Conclusions

The aim of the present study was to analyze the effect of the longitudinal movement on the performance of small-scale linear Fresnel reflectors at two European locations. Different configurations were analyzed and compared with the typical configuration of a large-scale linear Fresnel reflector. The available area for *SSLFR* installation divides the study into two possible scenarios: the available area is not a critical parameter (the energy absorbed by the absorber tube and the primary cost are evaluated), and the available area is a critical parameter (the reflector area ratio is evaluated).

The analysis has shown that the configurations that have two longitudinal movements (configuration C_2 and C_5) do not show good results of annual energy and they increase the primary cots, both in Almeria and in Berlin.

In Almeria, the longitudinal movements have a positive influence in the annual energy, with a moderate increase of the primary cost for the configurations whose longitudinal movements ensure the rays reflected by the mirrors in the longitudinal direction are always vertical for any time of day. The configurations whose longitudinal movements depend on the latitude show worse results than the typical configuration of a large-scale linear Fresnel reflector.

On the other hand, in Berlin, the longitudinal movements show a positive influence in the annual energy, but they imply a notable increase of the primary cost. The configurations whose longitudinal movements depend on the latitude also show good results for the annual energy absorbed, with a notable increase of the primary
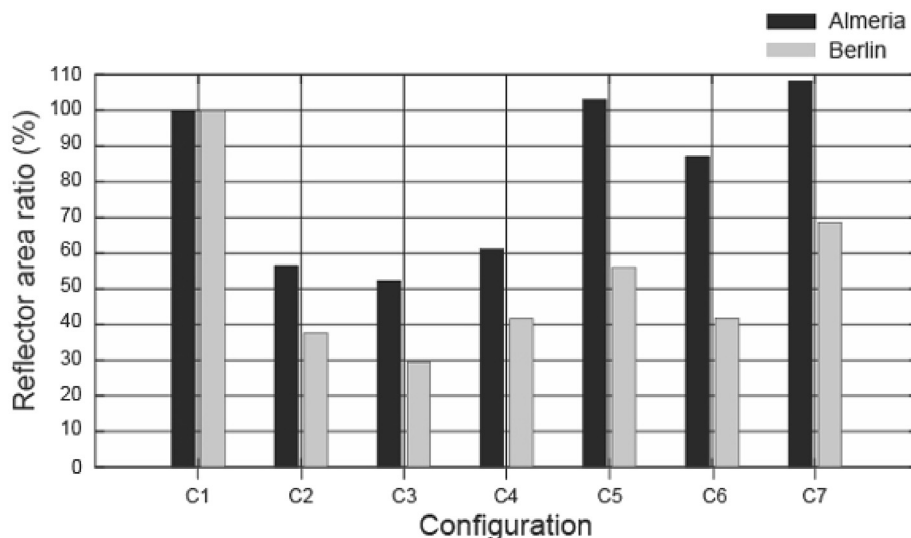
Fig. 10. Reflector area ratio.

cost.

In the configurations without longitudinal movement in the secondary reflector system, the inclination of the secondary reflector system has a noticeable effect on the results. The analysis shows that increasing the inclination of the secondary reflector system leads to an increase of the annual energy, with a moderate increase of the primary cost, in Almeria. On the contrary, in Berlin, this increase implies a considerable increase of the annual energy and the primary cost.

The results of this study indicate that, in terms of the energy absorbed by the absorber tube and the primary cost, the best behavior is obtained for configuration C_3, in Almeria and Berlin. The analysis has shown that the configurations whose longitudinal movements depend on the latitude, have better results for geographic location with greater latitude.

The analysis has shown that in the configurations whose longitudinal movements allow that the reflected rays by the mirrors in the longitudinal direction are always vertical for any time of day, the longitudinal movement reduces significantly the area required for *SSLFR* installation, with better results in Berlin than in Almeria. On the contrary, the configurations whose longitudinal movements depend on the latitude, show worst general results both in Almeria and in Berlin, being the results in Almeria notably worst. On this regard, the best behavior is obtained for configuration C_3 as well, for both locations.

Acknowledgments

References

[1] BP Statistical Review of World Energy, 2016.

[2] P. Río, C. Peñasco, P. Mir-Artigues, An overview of drivers and barriers to concentrated solar power in the European Union, Renew. Sustain. Energy Rev. 81 (2018) 1019–1029.

[3] Doha Amendment to the Kyoto Protocol, Adopted 8 December 2012, Decision 1/CMP 8 (2012). C.N.718.2012.TREATIES-XXVII.7.c.

[4] G. Zhu, T. Wendelin, M.J. Wagner, C. Kutscher, History, current state, and future of linear Fresnel concentrating solar collectors, Sol. Energy 103 (2014) 639–652.

[5] European Commission, Energy – Heating and cooling, from https://ec.europa.eu/energy/en/topics/energyefficiency/heating-and-cooling, accessed on 22 August 2017.

[6] C. Tzivanidis, E. Bellos, The use of parabolic trough collectors for solar cooling – a case study for Athens climate, Case Stud. Therm. Eng. 8 (2016) 403–413.

[7] B. Zou, J. Dong, Y. Yao, Y. Jiang, An experimental investigation on a small-sized parabolic trough solar collector for water heating in cold areas, Appl. Energy 163 (2016) 396–407.

[8] N. El Gharbia, H. Derbalb, S. Bouaichaouia, N. Said, A comparative study between parabolic trough collector and linear Fresnel reflector technologies, Energy Proced. 6 (2011) 565–572.

[9] R. Singh, Modeling and Performance Analysis of Linear Fresnel Collector for Process Heat Generation for Ice Cream Factory in Konya, MS Thesis, Middle East Technical University, 2017.

[10] A. Häberle, M. Berger, F. Luginsland, C. Zahler, M. Baitsch, H. Henning, M. Rommel, Linear concentrating Fresnel collector for process heat applications. Solar Paces, in: 13th International Symposium on Concentrating Solar Power and Chemical Energy Technologies, June 20–23, Sevilla, Spain, 2006.

[11] J. Rawlins, M. Ashcroft, Report: Small-Scale Concentrated Solar Power – a Review of Current Activity and Potential to Accelerate Employment, carbon trust, 2013.

[12] T. Sultana, G.L. Morrison, G. Rosengarten, Thermal performance of a novel rooftop solar micro-concentrating collector, Sol. Energy 86 (2012) 1992–2000.

[13] T. Sultana, G.L. Morrison, R.A. Taylor, G. Rosengarten, Numerical and experimental study of a solar micro concentrating collector, Sol. Energy 112 (2015) 20–29.

[14] G. Mokhtar, B. Boussad, S. Noureddine, A linear Fresnel reflector as a solar system for heating water: theoretical and experimental study, Case Stud. Therm. Eng. Case 8 (2016) 176–186.

[15] P. Bermejo, F.J. Pino, F. Rosa, Solar absorption cooling plant in Seville, Sol. Energy 84 (2010) 1503–1512.

[16] F.J. Pino, R. Caro, F. Rosa, J. Guerra, Experimental validation of an optical and thermal model of a linear Fresnel collector system, Appl. Therm. Eng. 50 (2013) 1463–1471.

[17] M.A. Serag-Eldin, Thermal design of a roof-mounted CLFR collection system for a desert absorption chiller, Int. J. Sustain. Energy 33 (2014) 506–524.

[18] N. Velázquez, O. García-Valladares, D. Sauceda, R. Beltrán, Numerical simulation of a linear Fresnel reflector concentrator used as direct generator in a solar-GAX cycle, Energy Convers. Manag. 51 (2010) 434–445.

[19] I.B. Askari, M. Ameri, Techno economic feasibility analysis of Linear Fresnel solar field as thermal source of the MED/TVC desalination system, Desalination 394 (2016) 1–17.

[20] A. Barbón, J.A. Sánchez-Rodríguez, L. Bayón, N. Barbón, Development of a fiber daylighting system based on a small-scale linear Fresnel reflector: theoretical elements, Appl. Energy 212 (2018) 733–745.

[21] J. Dai, H. Zheng, Y. Su, Z. Chang, The motional design and analysis for linear Fresnel reflector system combined three-movement, Energy Proced. 14 (2012) 971–976.

[22] A. Barbón, N. Barbón, L. Bayón, J.A. Otero, Theoretical elements for the design of a small-scale linear Fresnel reflector: frontal and lateral views, Sol. Energy 132 (2016) 188–202.

[23] A. Barbón, N. Barbón, L. Bayón, J.A. Otero, Optimization of the length and position of the absorber tube in small-scale Linear Fresnel Concentrators, Renew. Energy 99 (2016) 986–995.

[24] Y. Zhu, J. Shi, Y. Li, L. Wang, Q. Huang, G. Xu, Design and experimental investigation of a stretched parabolic linear Fresnel reflector collecting system, Energy Convers. Manag. 126 (2016) 89–98.

[25] Y. Zhu, J. Shi, Y. Li, L. Wang, Q. Huang, G. Xu, Design and thermal performances of a scalable linear Fresnel reflector solar system, Energy Convers. Manag. 146 (2017) 174–181.

[26] H. Bryan, H. Rallapalli, J. Jin Ho, Designing a solar ready roof: establishing the conditions for a high-performing solar installation, in: 39th ASES National Solar Conference, vol. 5, 2010, pp. 4081–4110.

[27] L. Bergamasco, P. Asinari, Scalable methodology for the photovoltaic solar energy potential assessment based on available roof surface area: application to Piedmont Region (Italy), Sol. Energy 85 (2011) 1041–1055.

[28] B. Giffith, P. Torcellini, N. Long, Assessment of the Technical Potential for Achieving Zero-Energy Commercial Buildings, ACEEE Summer Study Pacific Grove, 2006.

[29] A. Barbón, L. Bayón, N. Barbón, J.A. Otero, C. Bayón-Cueli, L. Rodríguez, F. Salgero, Concentrador solar lineal Fresnel con triple movimiento, Spain Patent ES 2601222 (B1) 2017.

[30] P. Kuzdzal, Solar collector having Fresnel mirrors, US Patent 9897344 (B2), 2018.

[31] G. Morin, J. Dersch, W. Platzer, M. Eck, A. Häberle, Comparison of linear Fresnel and parabolic trough collector power plants, Sol. Energy 86 (2012) 1–12.

[32] I. Reda, A. Andreas, Solar Position Algorithm for Solar Radiation Applications, 2008. Technical Report NREL/TP-560-34302, Colorado, USA.

[33] A. Barbón, N. Barbón, L. Bayón, J.A. Sánchez-Rodríguez, Parametric study of the small-scale linear Fresnel reflector, Renew. Energy 116 (2018) 64–74.

[34] J.A. Duffie, W.A. Beckman, Solar Engineering of Thermal Processes, fourth ed., John Wiley & Sons, New York, 2013.

[35] M. Binotti, G. Manzolini, G. Zhu, An alternative methodology to treat solar radiation data for the optical efficiency estimate of different types of collectors, Sol. Energy 110 (2014) 807–817.

[36] M.A. Moghimi, K.J. Craig, J.P. Meyer, A novel computational approach to combine the optical and thermal modelling of Linear Fresnel Collectors using the finite volume method, Sol. Energy 116 (2015) 407–427.

[37] V.M. Sharma, J.K. Nayak, S.B. Kedare, Effects of shading and blocking in linear Fresnel reflector field, Sol. Energy 113 (2015) 114–138.

[38] P.H. Theunissen, W.A. Beckman, Solar transmittance characteristics of evacuated tubular collectors with diffuse back reflectors, Sol. Energy 35 (1985) 311–320.

[39] A. Barbón, J.A. Sánchez-Rodríguez, L. Bayón, C. Bayón-Cueli, Cost estimation relationships of a small-scale linear Fresnel reflector, Renew. Energy (2018) (in press), https://doi.org/10.1016/j.renene.2018.09.060.

[40] PVGIS. Joint Research Centre (JRC, 2018. Available on line at, http://re.jrc.ec.europa.eu/pvgis/apps4/pvest.php.

[41] A. Barbón, N. Barbón, L. Bayón, J.A. Sánchez-Rodríguez, Optimization of the distribution of small-scale linear Fresnel reflectors on roofs of urban buildings, Appl. Math. Model. 59 (2018) 233–250.